Research Article | Vol. 25, No. 20 | 2 Oct 2017 | OPTICS EXPRESS 23567
Optics EXPRESS

Directional enhancement of selected high-order-harmonics from intense laser irradiated blazed grating targets

GUOBO ZHANG,[1,2] MIN CHEN,[1,3,5] FENG LIU,[1,3] XIAOHUI YUAN,[1,3] SUMING WENG,[1,3] JUN ZHENG,[1,3] YANYUN MA,[2,3,6] FUQIU SHAO,[2] ZHENGMING SHENG,[1,3,4] AND JIE ZHANG[1,3]

[1]*Key Laboratory for Laser Plasmas (MOE) and School of Physics and Astronomy, Shanghai Jiao Tong University, Shanghai 200240, China*
[2]*College of Science, National University of Defense Technology, Changsha 410073, China*
[3]*Collaborative Innovation Center of IFSA (CICIFSA), Shanghai Jiao Tong University, Shanghai 200240, China*
[4]*SUPA, Department of Physics, University of Strathclyde, Glasgow G4 0NG, UK*
[5]*minchen@sjtu.edu.cn*
[6]*yanyunma@126.com*

Abstract: Relativistically intense laser solid target interaction has been proved to be a promising way to generate high-order harmonics, which can be used to diagnose ultrafast phenomena. However, their emission direction and spectra still lack tunability. Based upon two-dimensional particle-in-cell simulations, we show that directional enhancement of selected high-order-harmonics can be realized using blazed grating targets. Such targets can select harmonics with frequencies being integer times of the grating frequency. Meanwhile, the radiation intensity and emission area of the harmonics are increased. The emission direction is controlled by tailoring the local blazed structure. Theoretical and electron dynamics analysis for harmonics generation, selection and directional enhancement from the interaction between multi-cycle laser and grating target are carried out. These studies will benefit the generation and application of laser plasma-based high order harmonics.

OCIS codes: (190.0190) Nonlinear optics; (350.5400) Plasmas; (190.4160) Multiharmonic generation; (350.2770) Gratings.

References and links

1. F. Krausz and M. Ivanov, "Attosecond physics," Rev. Mod. Phys. **81**(1), 163–234 (2009).
2. Z. Tao, C. Chen, T. Szilvási, M. Keller, M. Mavrikakis, H. Kapteyn, and M. Murnane, "Direct time-domain observation of attosecond final-state lifetimes in photoemission from solids," Science **353**(6294), 62–67 (2016).
3. H. Timmers, M. Sabbar, J. Hellwagner, Y. Kobayashi, D. M. Neumark, and S. R. Leone, "Polarization-assisted amplitude gating as a route to tunable, high-contrast attosecond pulses," Optica **3**(7), 707–710 (2016).
4. C. P. Zhang, C. L. Xia, X. F. Jia, and X. Y. Miao, "Multiple rescattering processes in high-order harmonic generation from molecular system," Opt. Express **24**(18), 20297–20308 (2016).
5. R. Lichters, J. Meyer-ter-Vehn, and A. Pukhov, "Shortpulse laser harmonics from oscillating plasma surfaces driven at relativistic intensity," Phys. Plasmas **3**(9), 3425–3437 (1996).
6. J. Zhang, M. Zepf, P. A. Norreys, A. E. Dangor, M. Bakarezos, C. N. Danson, A. Dyson, A. P. Fews, P. Gibbon, M. H. Key, P. Lee, P. Loukakos, S. Moustaizis, D. Neely, F. N. Walsh, and J. S. Wark, "Coherence and bandwidth measurements of harmonics generated from solid surfaces irradiated by intense picosecond laser pulses," Phys. Rev. A **54**(2), 1597–1603 (1996).
7. P. A. Norreys, M. Zepf, S. Moustaizis, A. P. Fews, J. Zhang, P. Lee, M. Bakarezos, C. N. Danson, A. Dyson, P. Gibbon, P. Loukakos, D. Neely, F. N. Walsh, J. S. Wark, and A. E. Dangor, "Efficient extreme UV harmonics generated from picosecond laser pulse interactions with solid targets," Phys. Rev. Lett. **76**(11), 1832–1835 (1996).
8. T. Baeva, S. Gordienko, and A. Pukhov, "Theory of high-order harmonic generation in relativistic laser interaction with overdense plasma," Phys. Rev. E Stat. Nonlin. Soft Matter Phys. **74**(4), 046404 (2006).
9. U. Teubner and P. Gibbon, "High-order harmonics from laser-irradiated plasma surfaces," Rev. Mod. Phys. **81**(2), 445–473 (2009).
10. C. Thaury and F. Quéré, "High-order harmonic and attosecond pulse generation on plasma mirrors: basic mechanisms," J. Phys. At. Mol. Opt. Phys. **43**(21), 213001 (2010).

#298015 https://doi.org/10.1364/OE.25.023567
Journal © 2017 Received 4 Jul 2017; revised 14 Sep 2017; accepted 14 Sep 2017; published 18 Sep 2017

Optics EXPRESS

11. M. Behmke, D. an der Brügge, C. Rödel, M. Cerchez, D. Hemmers, M. Heyer, O. Jäckel, M. Kübel, G. G. Paulus, G. Pretzler, A. Pukhov, M. Toncian, T. Toncian, and O. Willi, "Controlling the Spacing of Attosecond Pulse Trains from Relativistic Surface Plasmas," Phys. Rev. Lett. **106**(18), 185002 (2011).
12. C. Rödel, D. an der Brügge, J. Bierbach, M. Yeung, T. Hahn, B. Dromey, S. Herzer, S. Fuchs, A. G. Pour, E. Eckner, M. Behmke, M. Cerchez, O. Jäckel, D. Hemmers, T. Toncian, M. C. Kaluza, A. Belyanin, G. Pretzler, O. Willi, A. Pukhov, M. Zepf, and G. G. Paulus, "Harmonic Generation from Relativistic Plasma Surfaces in Ultrasteep Plasma Density Gradients," Phys. Rev. Lett. **109**(12), 125002 (2012).
13. B. Dromey, S. Rykovanov, M. Yeung, R. Hörlein, D. Jung, D. C. Gautier, T. Dzelzainis, D. Kiefer, S. Palaniyppan, R. Shah, J. Schreiber, H. Ruhl, J. C. Fernandez, C. L. S. Lewis, M. Zepf, and B. M. Hegelich, "Coherent synchrotron emission from electron nanobunches formed in relativistic laser–plasma interactions," Nat. Phys. **8**(2439), 804–808 (2012).
14. Z. Y. Chen and A. Pukhov, "Bright high-order harmonic generation with controllable polarization from a relativistic plasma mirror," Nat. Commun. **7**, 12515 (2016).
15. Z. M. Sheng, K. Mima, J. Zhang, and H. Sanuki, "Emission of Electromagnetic Pulses from Laser Wakefields through Linear Mode Conversion," Phys. Rev. Lett. **94**(9), 095003 (2005).
16. C. Thaury, F. Quéré, J. P. Geindre, A. Levy, T. Ceccotti, P. Monot, M. Bougeard, F. Réau, P. D'oliveira, P. Audebert, R. Marjoribanks, and Ph. Martin, "Plasma mirrors for ultrahigh-intensity optics," Nat. Phys. **3**(6), 424–429 (2007).
17. F. Quéré, C. Thaury, P. Monot, S. Dobosz, P. Martin, J. P. Geindre, and P. Audebert, "Coherent Wake Emission of High-Order Harmonics from Overdense Plasmas," Phys. Rev. Lett. **96**(12), 125004 (2006).
18. M. Bocoum, M. Thévenet, F. Böhle, B. Beaurepaire, A. Vernier, A. Jullien, J. Faure, and R. Lopez-Martens, "Anticorrelated Emission of High Harmonics and Fast Electron Beams From Plasma Mirrors," Phys. Rev. Lett. **116**(18), 185001 (2016).
19. S. Gordienko, A. Pukhov, O. Shorokhov, and T. Baeva, "Relativistic Doppler Effect: Universal Spectra and Zeptosecond Pulses," Phys. Rev. Lett. **93**(11), 115002 (2004).
20. G. D. Tsakiris, K. Eidmann, J. Meyer-ter-Vehn, and F. Krausz, "Route to intense single attosecond pulses," New J. Phys. **8**(1), 19 (2006).
21. P. Heissler, R. Hörlein, J. M. Mikhailova, L. Waldecker, P. Tzallas, A. Buck, K. Schmid, C. M. S. Sears, F. Krausz, L. Veisz, M. Zepf, and G. D. Tsakiris, "Few-Cycle Driven Relativistically Oscillating Plasma Mirrors: A Source of Intense Isolated Attosecond Pulses," Phys. Rev. Lett. **108**(23), 235003 (2012).
22. M. Yeung, B. Dromey, S. Cousens, T. Dzelzainis, D. Kiefer, J. Schreiber, J. H. Bin, W. Ma, C. Kreuzer, J. Meyer-ter-Vehn, M. J. V. Streeter, P. S. Foster, S. Rykovanov, and M. Zepf, "Dependence of Laser-Driven Coherent Synchrotron Emission Efficiency on Pulse Ellipticity and Implications for Polarization Gating," Phys. Rev. Lett. **112**(12), 123902 (2014).
23. S. Cousens, B. Reville, B. Dromey, and M. Zepf, "Temporal Structure of Attosecond Pulses from Laser-Driven Coherent Synchrotron Emission," Phys. Rev. Lett. **116**(8), 083901 (2016).
24. S. Kahaly, S. Monchocé, H. Vincenti, T. Dzelzainis, B. Dromey, M. Zepf, P. Martin, and F. Quéré, "Direct Observation of Density-Gradient Effects in Harmonic Generation from Plasma Mirrors," Phys. Rev. Lett. **110**(17), 175001 (2013).
25. X. Cao, S. Jiang, C. Yu, Y. Wang, L. Bai, and R. Lu, "Generation of isolated sub-10-attosecond pulses in spatially inhomogenous two-color fields," Opt. Express **22**(21), 26153–26161 (2014).
26. P. Zhang and A. G. R. Thomas, "Enhancement of high-order harmonic generation in intense laser interactions with solid density plasma by multiple reflections and harmonic amplification," Appl. Phys. Lett. **106**(13), 131102 (2015).
27. M. Yeung, S. Rykovanov, J. Bierbach, L. Li, E. Eckner, S. Kuschel, A. Woldegeorgis, C. Rödel, A. Sävert, G. G. Paulus, M. Coughlan, B. Dromey, and M. Zepf, "Experimental observation of attosecond control over relativistic electron bunches with two-colour fields," Nat. Photonics **11**(239), 32–35 (2016).
28. M. R. Edwards and J. M. Mikhailova, "Waveform-Controlled Relativistic High-Order-Harmonic Generation," Phys. Rev. Lett. **117**(12), 125001 (2016).
29. M. Yeung, M. Zepf, M. Geissler, and B. Dromey, "Angularly separated harmonic generation from intense laser interaction with blazed diffraction gratings," Opt. Lett. **36**(12), 2333–2335 (2011).
30. K. Q. Pan, C. Y. Zheng, and X. T. He, "Surface plasma waves with their harmonics generation from pre-structured targets," Phys. Plasmas **23**(2), 023109 (2016).
31. L. Fedeli, A. Sgattoni, G. Cantono, and A. Macchi, "Relativistic surface plasmon enhanced harmonic generation from gratings," Appl. Phys. Lett. **110**(5), 051103 (2017).
32. X. Lavocat-Dubuis and J. P. Matte, "Numerical simulation of harmonic generation by relativistic laser interaction with a grating," Phys. Rev. E Stat. Nonlin. Soft Matter Phys. **80**(5), 055401 (2009).
33. X. Lavocat-Dubuis and J. P. Matte, "Numerical and theoretical study of the generation of extreme ultraviolet radiation by relativistic laser interaction with a grating," Phys. Plasmas **17**(9), 093105 (2010).
34. S. J. Zhang, H. B. Zhuo, D. B. Zou, L. F. Gan, H. Y. Zhou, X. Z. Li, M. Y. Yu, and W. Yu, "Model of high-order harmonic generation from laser interaction with a plasma grating," Phys. Rev. E Stat. Nonlin. Soft Matter Phys. **93**(5), 053206 (2016).
35. S. Kahaly, S. K. Yadav, W. M. Wang, S. Sengupta, Z. M. Sheng, A. Das, P. K. Kaw, and G. R. Kumar, "Near-Complete Absorption of Intense, Ultrashort Laser Light by Sub-Lambda Gratings," Phys. Rev. Lett. **101**(14), 145001 (2008).

Optics EXPRESS

36. M. Blanco, M. T. Flores-Arias, C. Ruiz, and M. Vranic, "Table-top laser-based proton acceleration in nanostructured targets," New J. Phys. **19**(3), 033004 (2017).
37. M. Chen, N. Kumar, A. Pukhov, and T. P. Yu, "Stabilized radiation pressure dominated ion acceleration from surface modulated thin-foil targets," Phys. Plasmas **18**(7), 073106 (2011).
38. M. Cerchez, A. L. Giesecke, C. Peth, M. Toncian, B. Albertazzi, J. Fuchs, O. Willi, and T. Toncian, "Generation of Laser-Driven Higher Harmonics from Grating Targets," Phys. Rev. Lett. **110**(6), 065003 (2013).
39. M. Hutley, Diffraction Gratings (Academic, 1982).
40. M. Yeung, B. Dromey, C. Rödel, J. Bierbach, M. Wünsche, G. Paulus, T. Hahn, D. Hemmers, C. Stelzmann, G. Pretzler, and M. Zepf, "Near-monochromatic high-harmonic radiation from relativistic laser–plasma interactions with blazed grating surfaces," New J. Phys. **15**(2), 025042 (2013).
41. R. A. Fonseca, L. O. Silva, F. S. Tsung, V. K. Decyk, W. Lu, C. Ren, W. B. Mori, S. Deng, S. Lee, T. Katsouleas, and J. C. Adam, "OSIRIS: A three-dimensional fully relativistic particle in cell code for modeling plasma based accelerators," Lect. Notes Comput. Sci. **2331**, 342–351 (2002).

1. Introduction

Ultra-short intense extreme ultraviolet (XUV) pulses are very useful for detecting micro-dynamics of atoms, molecular and condensed matter [1,2]. High-order harmonics generated from non-relativistic intense laser interaction with noble gases are typical XUV sources, which have been widely used [3,4]. However, the intensities of these harmonics are restricted by the low driver intensity. With higher laser intensity, electron recombination process is inhibited and the high-order harmonics from laser irradiated gas target is inefficient. Recently researches demonstrate that, intense high-order harmonics generation (HHG) can be obtained from solid targets driven by relativistically intense laser. In the last two decades, great efforts have been made to generate controllable intense harmonics through this scheme [5–14]. Hitherto, there are two main mechanisms contributing to the high-order harmonic generation, i.e. coherent wake emission (CWE) and relativistic oscillating mirror (ROM). The CWE mechanism works well in weakly-relativistic laser intensities, which excites high-frequency plasma oscillations in the plasma density gradient by Brunel-heated electrons. Through the mode conversion processes [15,16], the electrostatic plasma wave can be converted to electromagnetic waves [17,18]. The ROM mechanism occurs when the target surface electrons are excited and relativistically oscillated by the driver pulse. The Doppler effects make the reflected pulse from these oscillating mirrors as ultrashort pulse trains with high-order harmonic component [8,19–21]. Recently, a new HHG mechanism namely coherent synchrotron emission (CSE) was reported, which occurs when a *p*-polarized laser incidents obliquely on a target. A dense electron nano-bunch is dragged out behind the target thereby generating harmonics [13,22,23]. Theoretical and experimental studies have been carried out to investigate the efficiency of these mechanisms. However, the efficiency of HHG from such intense laser solid target interaction is still low, especially when the target surface is too smooth. Some improved schemes to enhance the conversion efficiency have been proposed, such as using pre-pulse to optimize the density scale length [11,12,24], using two-color or multi-color light to control the waveform of driver pulses [25–28], and using microstructure target to enhance the coherent radiation intensity [29–34].

Among them using microstructure grating target is a relatively simple way to get intensively enhancement of specific orders of harmonics. Previous studies have already shown that a grating target can be used to increase the energy conversion efficiency into hot electrons and ions [35–37]. For HHG, depending on the ratio of the grating structure period to the driver pulse wavelength, the target can be divided into two categories, wavelength scale or sub-wavelength scale. The wavelength scale target can resonantly excite surface plasma waves (SPW) when the incidence angle of the driver pulse is matched with the structure period, i.e. $\sin(\theta_{res}) \approx -1 + n\lambda_0/d$, where θ_{res} is the resonant angle of incidence, λ_0 is the laser wavelength, n is an integer number and d is the grating period [30,31]. For sub-wavelength scale target, selected orders of harmonics can be produced close to the grating surface with radiation wavelength λ_r satisfying [32–34]:

Optics EXPRESS

$$n\lambda_r/d = \cos(\alpha) - \sin(\theta_i) \quad (1)$$

where α and θ_i represent the observation and incidence angles, respectively. The HHG enhancement from such periodically modulated targets has already been demonstrated in experiments [38].

Blazed diffraction grating is a special kind of grating target, which is widely used in optical spectrum measurement to enhance the spectrum brightness along a controllable direction [39]. In previous work, both numerical simulations and experiments have demonstrated that selected harmonics can be obtained from relativistic laser-plasma interactions with blazed grating targets when an appropriate blaze condition is satisfied, which provides a potential route to achieve near-monochromatic, short pulsed XUV radiation [29,40]. In this paper, we revisited the HHG from blazed grating targets and show that such targets cannot only select the specific harmonics in a specific direction through grating diffraction, but also enhance the maximum detectable harmonic order and intensity in a predetermined direction. This kind of enhancement is attributed to the coherent addition effects resulted from grating structure and stronger electron acceleration around a single grating protuberance. Our studies also show that in comparison to normal gratings such as with rectangular protuberances structures, the blazed grating with triangular structures can change the local incidence angle of the driver laser determined by the groove shape. So this blazed structure can yield higher energy absorption of electrons and enhance the harmonic intensity in the predetermined direction.

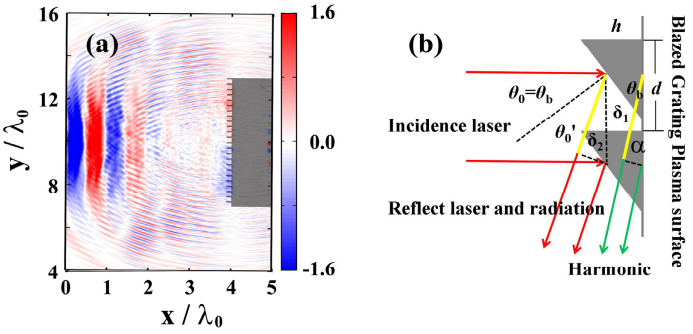

Fig. 1. (a) Transverse magnetic fields of driver laser and high-order harmonics from a normally incident laser pulse interaction with a grating target, the color bar is normalized by $mc\omega_0/e$. (b) Schematic of HHG from blazed grating surface. Here *d* is the grating period, *h* is the groove depth, θ_b, θ_0, θ_0' are the blazed angle, incidence angle and diffraction angle, respectively. Here $\theta_b=\theta_0=\theta_0'$, δ_1 and δ_2 are the optical path differences at the reflected radiation and surface harmonic, α is the harmonic emission angle.

2. Simulation of HHG from normal grating targets

To study high-order harmonic generation from an ultra-intense laser pulse irradiated grating targets, we performed a series of two-dimensional (2D) particle-in-cell (PIC) simulations by using the OSIRIS code [41]. The schematic view of our studies is shown in Fig. 1(a) and the typical structure of a blazed grating target and the laser incidence are shown in Fig. 1(b). A linearly polarized (p-polarized) laser pulse with wavelength of λ_0=800nm irradiates the targets along the normal direction as shown in Fig. 1(b). The normalized laser electric field is given by $a = eE/m\omega_0 c = a_0 \sin^2(\pi t/\tau)\exp(-y^2/w_0^2)$, where e and m denote the charge and rest-mass of the electron, $\tau=6T_0=6\lambda_0/c$, $w_0=3\lambda_0$ is the laser spot radius, and the

Optics EXPRESS

dimensionless amplitude of the electric field is a_0=4, which corresponds to a peak laser intensity of I=3.4×10^{19} W/cm^2. To show the effects of a blazed grating target on HHG more clearly, we first study the laser normal grating target interaction and later we compare these result with the blazed target case. The normal grating target is $6\lambda_0$ wide and λ_0 thick with rectangular protuberance structure. The grating period is $d=\lambda_0/4$ and we define the grating frequency as $\omega_d=4\omega_0$. The depth of the grating protuberance is $h=\lambda_0/8$, the width of the protuberance is $\lambda_0/16$. The initial plasma density is $n_e=20n_c$, where n_c=1.1×10^{21}/$\lambda_0^{\,2}$ (μm^{-3}) is the critical plasma density for the incident laser pulse, and ions are immobile in the simulations. The simulation box is $5\lambda_0\times20\lambda_0$ with cell size $\lambda_0/250$ and 16 macro-particles per cell.

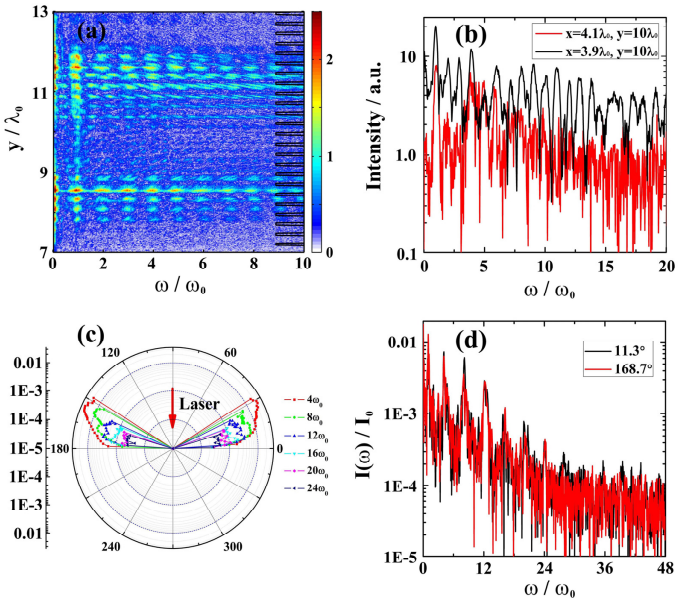

Fig. 2. (a) The transverse distribution of electric current $J_y(\omega,y)$ at $x=3.8\lambda_0$, and the black line shows the grating structure. (b) The transverse current spectra collected at two different positions: $x=3.9\lambda_0$, $y=10\lambda_0$ (inside the protuberance of grating target), and $x=4.1\lambda_0$, $y=10\lambda_0$ (inside the substrate of the grating target). The radiation angular distribution and typical far-field radiation spectra are shown in (c) and (d). All harmonic intensity here is normalized by the maximum intensity of the incident laser I_0 in the paper.

The spectral distribution of the electric current $J_y(\omega,y)$ at $x=3.8\lambda_0$ (near the grating surface) is shown in Fig. 2(a), where harmonic components with all integer times of the laser frequency can be clearly seen. The intensity distribution of harmonics is approximately symmetrical about the laser propagation axis ($y=10\lambda_0$), and the high-order harmonics is absent along this direction due to the too strong laser intensity there making the electrons move forward and the currents exist mainly inside the protuberance. Figure 2(b) shows the transverse current spectra $J_y(\omega,y)$ collected at two different longitudinal positions: one is inside the grating protuberances (black line) and the other is inside the substrate of the grating target (red line). We can see that the harmonic currents inside the substrate is much weaker than those in

Optics EXPRESS

the protuberance. Therefore, the harmonics mainly come from protuberances and each of them can be viewed as a source of radiation. The final radiation is the coherent addition of radiations from multiple periodic protuberances within the laser focus. This coherent effect makes only the radiations along the grating surface are constructively enhanced. The selected harmonics enhancement can be seen from the radiation angular distribution. Only the $4n\omega_0$ -order harmonics can be radiated along the grating surface, and other harmonic components are absent. The intensity is approximately symmetrically distributed, and typical radiation spectra at 11.3° and 168.7° are shown in Fig. 2(d) verifying this symmetry.

3. Directional enhancement of harmonic emissions from blazed grating targets

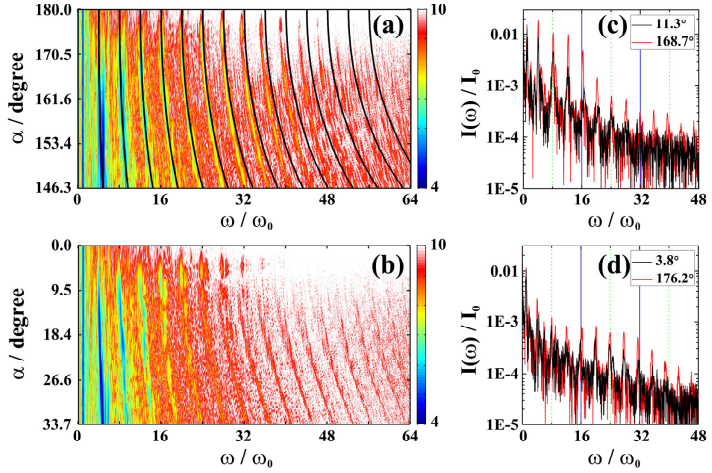

Fig. 3. Angular distributions of high-order harmonics around the reflection direction (a) and around the non-reflection direction (b) from a laser irradiated blazed grating target with $\theta_b = 40^\circ$. The black lines shown in (a) are from theoretical calculations. The color bars are normalized by $-\log P(\omega)$. (c) and (d) are the radiation spectra collected along two sets of symmetric directions.

As we show before, selected harmonic emissions with frequencies being integer times of the grating frequency can be enhanced along the target surface when normal grating targets are used, and other harmonic components are absent, especially for the higher order harmonics. For a blazed grating target, the surface enhancement will be stronger. We use the blazed angle $\theta_b = 40^\circ$, and keep the other parameters the same as normal grating target. Figures 3(a) and 3(b) show the spectra distributions of the emitted transverse electric fields $E_y(\omega, y)$ within two observation regions, i.e. the reflection direction (RD, Fig. 3(a)) and the non-reflection direction (NRD, Fig. 3(b)) of the incident laser pulse. The harmonics generated from such blazed grating target have four features. Firstly, only harmonics with frequencies of $4n\omega_0$ can be generated. Secondly, the harmonic emission is mainly along the surface of the blazed grating target. Thirdly, the radiation peak frequencies of the harmonics shift with the observation angle leading to the existence of non-integer order harmonics. Lastly, the harmonic spectra along the RD are stronger than along the NRD. The first three features are mainly due to the coherent addition effects of the radiations from multiple protuberances, which is similar as the normal grating target. The constructive interference from protuberances is satisfied with a relationship of the harmonic emission angle (α) and emission frequency (ω):

$$\cos(\alpha) = 4n\omega_0/\omega \tag{2}$$

Optics EXPRESS

The calculated curves from this relationship for different harmonics are plotted with black lines in Fig. 3(a). The peak frequency shifts agree with these theoretical estimations very well. The higher order of the harmonic corresponds to a larger frequency shifts within the unit angle difference. This provides a simple way to obtain harmonics with tunable frequency.

For the last feature, it is a combination of the coherent addition effects and the single protuberances enhancement effects. Radiations at two symmetric observation angles are compared in Figs. 3(c) and 3(d). One can clearly see that the harmonics intensity along RD is larger than that along NRD, and higher order harmonics can be generated along RD. For instance, the highest order of detectable harmonics is 32th along the NRD, but 48th harmonic along the RD can still be distinguished.

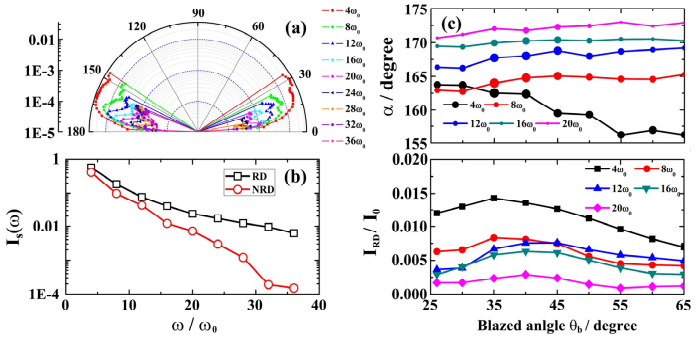

Fig. 4. (a) Angular distributions of harmonics from the blazed grating target. (b) Angularly integrated harmonic intensity I_2 along two symmetric directions. (c) Optimal angles with strongest harmonics emission as a function of the blazed angle. The point sizes represent the relative intensity of the harmonics. (d) Evolution of normalized harmonics intensity with emission angle of 168.7° along with the grating's blazed angle.

To show the directional enhancement of HHG from blazed grating target more clearly, we plot the angular distributions of each harmonics in Fig. 4(a). One can see that the emission region along the RD is larger than that along the NRD. For higher order harmonics, the emission direction is more close to the grating surface, which is consistent with the previous studies [32,33]. The total emission intensity $I_s(\omega_i) = \int_{\theta_1}^{\theta_2} I(\omega_i) d\theta$ within the RD and the NRD regions are shown in Fig. 4(b), which also confirms the harmonics enhancement along the RD. For example, the total intensities of the 32th and 36th harmonics along the RD have been enhanced for more than two orders of magnitude. Compared with the normal grating structure, this kind of directional enhancement is also obvious. We changed the blazed angle to see the optimal angles for the strongest harmonics emission and see the variation of the normalized intensity of the harmonics emitted along a fixed direction. The results are shown in Figs. 4(c) and 4(d). Again from Fig. 4(c) one can see that for different blazed angles, the higher is the harmonics order, the closer is the emission to the grating surface. From the point sizes represented harmonics intensity, one can see except the 4th harmonic, the optimal blazed angle for strongest high harmonics emission is about 40°. As Fig. 4(d) shows that the optimal blazed angle for the harmonic emission at angle of 168.7° is also 40°. Furthermore, comparing the intensity ratio between the emission along the RD and NRD at symmetric angles (not shown here), we found that the harmonics distributions are mainly concentrated in the reflection region and the maximum ratio is achieved when the blazed angle is also 40°. If the blazed angle exceeds 45°, the enhancement along the RD reduces. When the blazed angle is beyond 60°, the harmonics emission tends to be identical between the two directions.

Optics EXPRESS

4. Physical explanation of the directional enhancement emission

4.1. General theory and properties of HHG from multi-cycle laser interaction with grating targets

In this section, we use a simple model to analyze the properties of HHG from the grating targets. We start from a multi-cycle laser interaction with a solid plane target. As the consecutive laser cycle irradiates the target and the electromagnetic wave emits, one can receive the emitted signal $S(t)$ at a far-field fixed position (x, y). If we record the signal after the first laser cycle interaction as $f(t)$ and assume that the target can recover to the initial state immediately after each cycle's interaction, i.e. the successive cycles always interact with the same target surface. Then the total received signal can be expressed as:

$$S(t)=f(t)+f(t-T_0)+f(t-2T_0)+\ldots+f(t-NT_0)=\sum_0^N f(t-nT_0) \tag{3}$$

The final spectrum of the emitted signal is:

$$I(\omega)=F\left[S(t)\right]=\tilde{f}(\omega)\sum_0^N e^{i\omega nT_0} \tag{4}$$

Where F is the Fourier transformation opetator, $\tilde{f}(\omega)$ is the Fourier transformation of the emitted signal $f(t)$ and it respresents the spectrum resulting from single cycle laser target interaction, which is determined by the single cycle waveform and target response function. However, if the target cannot recover after each cycle interaction, it introduces a deformation factor $e^{i\alpha_n t}$ to the emitted signal and the initial target deformation is α_0=0. Then the frequency spectrum of the emitted signal becomes:

$$I(\omega)=\tilde{f}(\omega)\sum_0^N e^{i\omega nT_0+i\alpha_n} \tag{5}$$

Usually, $\tilde{f}(\omega)$ shows a broad spectrum, and the narrower is the target temporal response to the laser cycle, the larger is the cutoff frequency ($\omega_{\max}$) of the signal. The summation term $\sum_0^N e^{i\omega nT_0+i\alpha_n}$ shows the coherent addition effect from each laser cycle. If $e^{i\alpha_n t}$=1, the signal from each laser cycle is phase locked and the coherent effect takes maximum. The final spectrum shows harmonic peaks on the broad spectrum. $\tilde{f}(\omega)$ The larger is the number of the laser period (*N*), the narrower and stronger is each harmonic peak. In reality, the term $e^{i\alpha_n t}$ usually breaks phase locking, which may come from the target deformation, laser intensity difference between each cycle or laser frequency chirping.

Similarly, for the case of grating targets, we assume that the detected signal from single protuberance is $f_g(t)$, and take the optical path differences of each harmonic emission for laser normal incidence as $\delta_m = md\cos(\alpha)$. Substitute them into Eq. (3), the final harmonics spectrum can be expressed as:

$$I_g(\omega)=F\left(\sum_0^M f_g(t-\delta_m/c)\right)=\tilde{f}_g(\omega)\sum_0^M e^{im\omega d\cos(\alpha)/c} \tag{6}$$

Where the $\tilde{f}_g(\omega)$ respresents harmonic signal resulting from multi-cyle laser interaction with single protuberance, and it contains all of the harmonic components which corresponds to Fig. 2(b). The term $\sum_0^M e^{im\omega d\cos(\alpha)/c}$ determines the selected harmonics by the construction

Optics EXPRESS

interference of multi-protuberances. When the number of protuberances within the laser focus (M) is large enough and the exponential term $\omega d\cos(\alpha)/c$ is integer, then the radiation wavelength λ_r satisfying $n\lambda_r/d=\cos(\alpha)$, which is consistent with our previous simulation results. The final spectrum selects harmonic peaks from the multiple peak spectrum $\tilde{f}_g(\omega)$ which itself has peak structures on a broad spectrum $\tilde{f}(\omega)$. We point out that the phase mis-locking between each protuberance has not been considered yet, whose contribution breaks the coherent addition of each protuberance in a similar way as the term $e^{i\alpha_n t}$ breaking the coherent addition of each laser cycle.

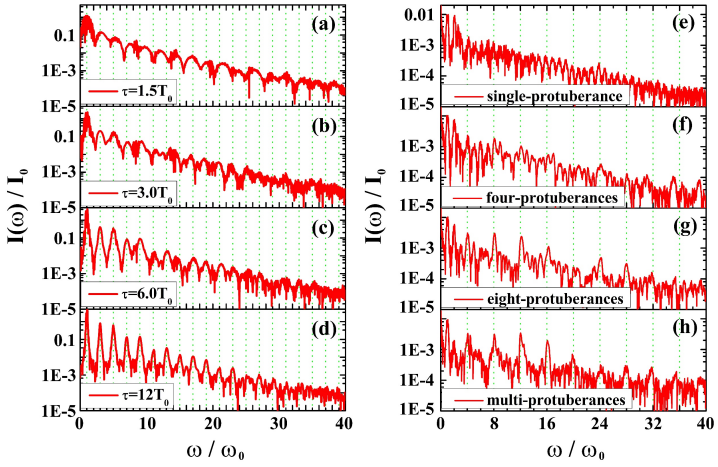

Fig. 5. The radiation spectra collected at reflected direction from a plane target interaction with lasers of different cycle numbers (a)-(d). The radiation spectra collected at 7.6° from grating targets with different protuberance numbers (e)-(h).

To verify the above analysis, we carry out simulations by using a p-polarized laser pulse normally incident on a plane target. Figures 5(a)-5(d) show the reflection spectra of laser pulses with different cycle numbers. By comparing the spectra, one can see a clear transition from a broad spectrum to harmonic characteristic with only odd orders [5]. The intensity scaling is basically determined by the single-cycle laser target interaction, as show in Fig. 5(a). The radiated harmonic spectrum gradually becomes distinct, and the peak intensity is enhanced and the width becomes narrower with the increase of laser cycle numbers due to the phase locked coherent addition as shown in Figs. 5(b)-5(d).

For grating targets, the radiation spectrum from the multi-cycle laser interaction with single and multiple protuberances are shown in Figs. 5(e)-5(h). The harmonics with integer times of laser frequencies can be seen for the case of single protuberance, which is denoted by the $\tilde{f}_g(\omega)$ term in Eq. (6). By comparing the harmonics spectra in Figs. 5(e)-5(f), one can find that the spectrum selection becomes evident with the increase of protuberance numbers. Finally, only harmonics with grating frequency are coherently enhanced. This is consistent with our theoretical analysis.

4.2. Dynamical analysis of HHG from grating targets

The above theoretical analysis of HHG is mainly focused on the temporal and spatial coherent addition effects on the final radiation signal, which is important to the peak characteristic of the spectrum. However, the final spectrum also depends on the single-cycle target response

Optics EXPRESS

function $f_g(t)$, which usually determines the cutoff frequency and the intensity scaling of the spectrum. Obviously, the target response function depends on the specific harmonic generation mechanism. Our studies show the HHG from the grating target is quite different from the previous ROM mechanism [5,8,19]. For grating targets, it is difficult to produce regular oscillating electron sheet due to the discontinuous and small protuberance structure along the transverse direction, which makes the laser energy absorption and the electron motion completely different from the plane target.

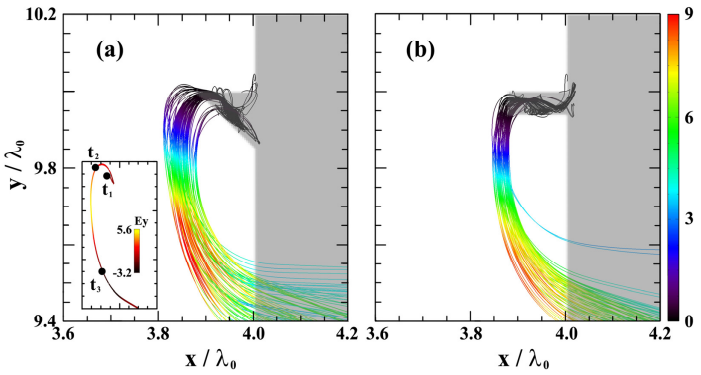

Fig. 6. Typical trajectories of representative electrons from the incline surface of a blazed grating (a) and a normal grating (b) targets with only single protuberance. The temporal duration of the trajectories is from t = 4.2 T_0 to t = 6.4 T_0. The color bar of trajectories represents the electrons energy γ. The inset in (a) shows the acceleration and radiation period of a single grating target electron, the color bar represents the transverse electric fields felt by the electron, which is normalized by $mc\omega_0/e$. The gray regions show the initial profiles of the two targets.

To understand the physics of the higher cutoff frequency and directional enhancement of HHG from the blazed grating target, typical electron trajectories from single protuberance grating during downward movement are shown in Figs. 6(a) and 6(b). The inset in Fig. 6(a) shows the acceleration and radiation processes of a typical grating target electron. When the ultra intense laser interacts with a grating target, the electrons inside the front area of the protuberances firstly move forward due to the laser ponderomotive force. The electrons inside the protuberances then move back along the lateral surface due to the charge separation force formed by the forward moving electrons and the left ions between t_1 and t_2. These electron can be stripped out forming a bunch. After being stripped out, the motions of the electrons in the vacuum gap are dominated by the laser fields. The momentum evolution satisfies Lorentz equation $d\vec{p}/dt = e\left(\vec{E} + \vec{p}/\gamma mc \times \vec{B}\right)$, where γ is the relativistic factor, $\vec{E}$ and $\vec{B}$ are the electric and magnetic fields of the laser. Therefore, the normalized momenta of these electrons can be given as $p_x = a_0^2 \sin^2(\varphi)/2$ and $p_y = a_0 \sin(\varphi)$ [36], where φ is the laser phase. One can see that these electrons carry opposite transverse momenta within two successive half laser cycle. They move upward in the first half cycle and downward in the next half cycle,which makes harmonics emission also along different directions. Meanwhile, we found that the energies of these stripped electrons are initially very low (with $\gamma \approx 1.2$), and they can only emit low-frequency radiation at this stage. Only when the electrons are returned back by the electromagnetic field of the laser and have obtained enough energy from the laser fields during the excursion, they radiate high-order harmonics along the direction of motion between t_2 and t_3. After this, these electrons enter into the target and scatter in space. Comparing the typical electron trajectories from the two grating targets, the downward moving electrons from

Optics EXPRESS

the inclined surface of the blazed grating target can obtain larger energy after leaving the target. Then, these blazed grating target electrons can also experience longer motion in the laser fields and reach higher energy. As is well-known that, the radiation intensity positively correlates with the relativistic factor γ, and the characteristic frequency of synchrotron radiation scales cubically with γ Therefore, the maximum detectable order of harmonics is increased at the reflection direction of the blazed grating target.

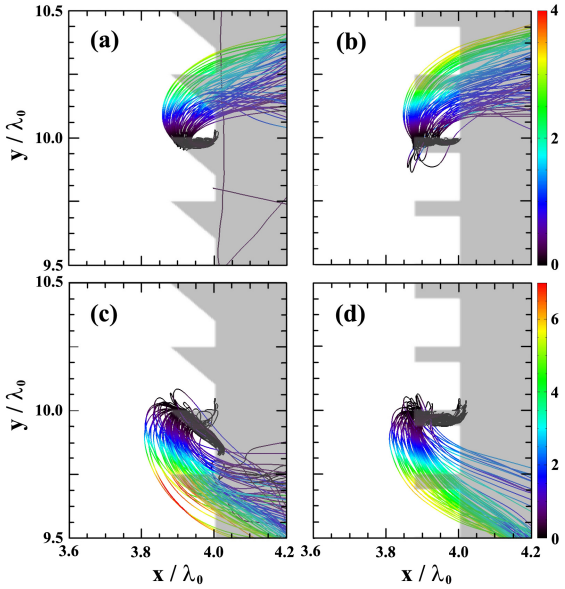

Fig. 7. Typical electron trajectories during the laser interaction with grating targets. The temporal duration of the trajectories in (a) and (b) is from t = 4.0 T_0 to t = 6.0 T_0. And the duration in (c) and (d) is from t = 4.2 T_0 to t = 6.4 T_0. The color bar of the trajectories represents the relativistic factor (γ) of the electrons.

The dynamical analysis of single protuberance also shows that during the laser-target interaction, electrons experience oscillating transverse momentum at different half cycle of the laser pulse. The upward and downward motion of electrons in blazed and normal grating targets with multiple protuberances are shown in Fig. 7. For the upward movement, the trajectories for the blazed and normal grating targets are similar. Nevertheless, for the downward movement, electrons from the blazed grating target obtain larger energy gain during the radiation process. And the electron bunch width in this case is also wider, which leads to enlarged emission region as shown in Fig. 4(a). In order to quantitatively show the energy differences, the evolutions of maximum electron energy in one periodic structure at the center of the two grating targets are shown in Fig. 8(a). The upward movement of electrons occurs at the half cycle points, and the downward movement of electrons occurs at the full cycle points. One can see that the maximum electron energy of upward movement is almost similar for the two targets. However, for the process of downward movement, the electron energy of the blazed grating is clearly larger than the normal grating target when the high fields part of the laser begins to irradiate the target around t=6T_0. Figure 8(b) shows the energy spectra of electrons from normal and blazed grating targets at t=6T_0. One can see that the number of high energy electrons with energy E>3MeV from a blazed grating target is larger than that from a normal grating target. The radiation intensity and the maximum detectable order of the harmonics are then be effectively enhanced in the blazed grating target case. These effects together with the temporal and spatial

Optics EXPRESS

coherent addition effects make the difference of the angular distribution and maximum cutoff frequency in the final spectra of the two grating targets.

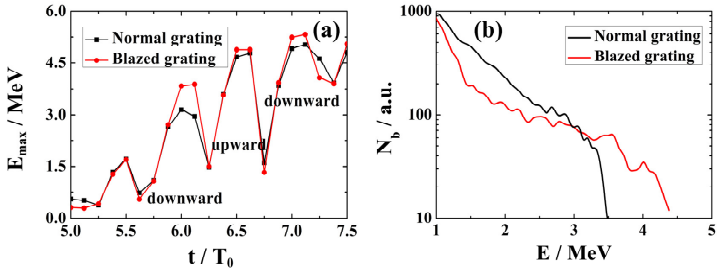

Fig. 8. (a) Evolution of the electrons maximum energy in the central protuberances of the targets. (b) Energy spectrum of the electrons from normal and blazed grating targets at $t=6T_0$

5. Summary and discussion

In summary, high-order harmonics generations by relativistic intense lasers interaction with blazed grating targets are investigated with 2D-PIC simulations. Such targets cannot only select harmonics with frequencies being multiple times of the grating frequency, but also enhances the radiation along the reflection direction of the blazed grating. Harmonics with higher maximum order can emit along this direction. These effects are due to the coherent addition effect of radiation from the grating surface and the enhancement effect from indidivual blazed protuberance which gives larger energy gain of the electrons. These studies will benefit the generation and application of laser plasma-based high order harmonics.

It deserves to point out that our general theory of HHG has separated the contributions of coherent effects from the single cycle response function $f(t)$. It shows that two different ways can be resorted to tune the final spectrum. We notice that recently by using two-color or multi-color laser driver scheme, Cao *et al* have tuned the single cycle response function to be much narrower in time, so the final cutoff frequency has been increased [25,27,28]. The blazed grating target studied here actually has used both the tuning effect of $f(t)$ and the spatial coherent addition effects. Besides these two effects, the de-coherence term $e^{i\alpha_n t}$ may also affect the final spectrum and may be controlled through laser chirping or pre-plasma tuning. More studies should be done to demonstrate its effectiveness and robustness.

Funding

The National Basic Research Program of China (Grant No. 2013CBA01504); The National Science Foundation of China (Grant Nos. 11374209, 11374210, 11475260, 11375265 and 11675264); Major State Basic Research Development Program of China (2015CB859700); Leverhulme Trust Research Project Grant and the U.K. EPSRC (Grant No. EP/N028694/1).

Acknowledgment

M. C. appreciates the support from National 1000 Youth Talent Project of China.